Pump power control of photon statistics in a nanowire quantum dot

Dan Dalacu ⬡,[*] David B. Northeast ⬡, Philip J. Poole ⬡, Geof C. Aers, and Robin L. Williams
National Research Council of Canada, Ottawa, Ontario, Canada K1A 0R6

Kim A. Owen and Daniel Oblak
*Department of Physics & Astronomy, Institute for Quantum Science and Technology, University of Calgary,
Calgary, Alberta, Canada T2N 1N4*

Through fluctuations in the local composition, InAsP quantum dots embedded within site-selected InP nanowires are observed to display biexciton binding energies spanning a range between -0.3 meV and $+2.9$ meV. From this range we select dots having energy-degenerate exciton and biexciton emission and observe an excitation rate-mediated transition from sub- to super-Poissonian second-order correlation statistics. Under pulsed excitation, $g^{(2)}(\tau = 0)$ is found to increase from 0.5 at high excitation levels, rising to 28 as the excitation is reduced by two orders of magnitude. The observed second-order correlation statistics are interpreted using both a stochastic model and a rate equation model of the competition between the various excitonic emission processes. Our results demonstrate that nanowire quantum dots represent a promising approach to the efficient generation of twin-photon states.

I. INTRODUCTION

The complex electronic structure of self-assembled semiconductor quantum dots has proven advantageous for the creation and manipulation of nonclassical states of light. The radiative decay of various excitonic complexes in such dots has been used to demonstrate single-photon emission [1–3], and the biexciton-exciton cascade [4] has been used to generate polarization-entangled pairs [5,6] and photon twins [7]. The states producing the quantum light can be finely engineered both during [8] and after growth [9], or they can be dynamically controlled using magnetic [6], electric [10], or strain fields [11].

The development of quantum light emitters based on bottom-up nanowire quantum dots [12] has paralleled that of strain-driven self-assembled dots [13], with the aim of producing a scalable technology based on single dots deterministically incorporated in site-controlled waveguides. These sources have demonstrated single photons with purities greater than 99% [14] and collection efficiencies greater than 40% [15]. Multipartite quantum states have also been demonstrated, including polarization-entangled pairs [16,17] and photon triplets [18]. As with self-assembled dots, the electronic levels can be finely tuned using growth conditions [19], postgrowth annealing [20], or dynamically using electric [21], magnetic [22], and strain fields [23].

In this work we investigate nanowire quantum dots that, depending on the microscopic composition of the dot, can demonstrate both positive and negative biexciton binding energies, $E_B = E_X - E_{XX}$, where E_X (E_{XX}) is the exciton

(biexciton) emission energy. In particular, we study the case of an energy-degenerate biexciton-exciton cascade where $E_B = 0$. This level alignment is relevant for the generation of polarization-entangled photon pairs in the presence of a fine-structure splitting (FSS) between the intermediate exciton states [24], i.e., the splitting due to anisotropic electron-hole exchange interaction [25]. The level alignment can also be used for generating photon twins, i.e., pairs of temporally correlated photons with identical energy and polarization [7]. Moreover, if such a source of photon twins were to be implemented using a symmetric quantum dot system (i.e., a dot with FSS = 0), generation rates could potentially be doubled as both polarizations of the emitted pairs of photons would be energy degenerate.

Here we focus on quantum dots for which both E_B and the FSS are equal to zero within our resolution limit. This system is studied using photon correlation measurements with both continuous-wave (cw) and pulsed excitation. We observe strong bunching up to 28 times (17 times) average probabilities in the low-excitation-rate limit for pulsed (cw) excitation, a signature of photon-twin generation. As the excitation rate is increased, we observe a transition to antibunched statistics with second-order correlation values of 0.5 (0.39) in the high-pump-rate limit for pulsed (cw) excitation. This excitation-rate-mediated transition from super- to sub-Poissonian statistics in the case of continuous-wave excitation is interpreted using calculations based on a four-level rate equation model which includes the biexciton state, the two bright exciton states, and the vacuum. In the case of pulsed excitation, the statistics are interpreted using a stochastic model to simulate the excitation-rate-dependent emission process.

---

[*]dan.dalacu@nrc.ca
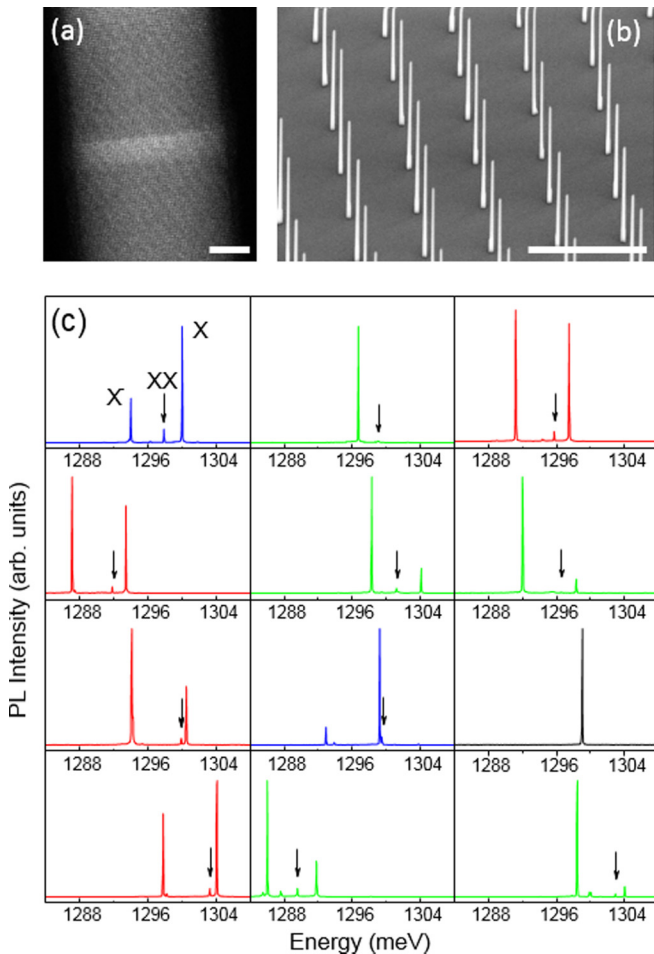
FIG. 1. (a) Transmission electron microscopy image of an InAsP quantum dot in an InP nanowire core. The scale bar is 5 nm. (b) Scanning electron microscopy image of a clad nanowire array. The scale bar is 10 μm. (c) PL spectra of 12 nanowires showing dominant X (blue), dominant X^- (green), and equally weighted (red) emissions as well as a single-peak spectrum (black) which may correspond to a degenerate $X - XX$ cascade (see text). Arrows indicate XX emission.

II. SAMPLE PREPARATION AND EXPERIMENTAL TECHNIQUES

The quantum dots were incorporated in site-controlled, bottom-up nanowires grown by selective-area vapor-liquid-solid epitaxy in the wurtzite InAs/InP material system. Using chemical beam epitaxy with trimethylindium, phosphine, and arsine as precursors for indium, phosphorus, and arsenic, respectively, growth was carried out on patterned InP substrates with single gold catalysts centered in circular openings in an SiO_2 mask (see Ref. [26] for details). Using a two-step growth process, a nanowire core was grown first into which was incorporated a single $InAs_xP_{1-x}$ dot [Fig. 1(a)] with a thickness of ~5 nm, a diameter of ~20 nm, and a composition of $x \sim 25\%$. In the second growth step, the nanowire core was clad with InP [14] and deliberately tapered [Fig. 1(b)]. This tapered geometry, inspired by work on top-down nanowires [27,28], produces devices with collection efficiencies of >40% [15]. Ground-state emission occurs at $\lambda \sim 950$ nm with near-transform-limited linewidths of 4 μeV

[15]. Owing to the high symmetry of the wurtzite {0001} system [29], mean FSSs are ~3 μeV [16].

Photoluminescence (PL) measurements were made in a closed-cycle helium cryostat at 4 K. The nanowire quantum dots were excited through a 100× objective (numerical aperture = 0.81) using either cw excitation (HeNe laser, $\lambda = 633$ nm) or pulsed excitation (diode laser, $\lambda = 670$ nm, pulse width = 100 ps). Emission was collected through the same microscope objective and directed to a 0.5-m grating spectrometer (resolution of 60 μeV) for detection with a liquid-nitrogen-cooled CCD. Second-order correlation measurements were made in a Hanbury Brown–Twiss configuration with the emission filtered using an angle-tuned interference filter (bandwidth = 2 nm) and detected using two single-photon avalanche photodiodes (APDs) with timing jitters of 200 ps.

III. RESULTS

In Fig. 1(c) we show the PL spectra obtained from 12 nanowires arrayed as in Fig. 1(b). The spectra show one to three peaks with resolution-limited linewidths of 60 μeV. Due to the small FSS between the neutral excitonic states mentioned above, distinguishing between charged and neutral complexes based on polarization is difficult. Instead, we rely on cross-correlation measurements [4] between the different emission peaks made on similar nanowire samples [15]. These measurements show that most low-excitation-power spectra consist of two peaks separated by ~5 meV which are associated with emission from the neutral exciton X (high-energy peak) and negatively charged exciton X^- (low-energy peak). The intensity ratio between these two peaks is nanowire dependent, varying from mostly X (blue curves) to mostly X^- (green curves), but is typically roughly equally weighted (red curves).

The biexciton XX is indicated in Fig. 1(c) by the black arrows and typically appears between X and X^- with a positive biexciton binding energy, $E_B > 0$, but dots with negative E_B are also observed (see third row, middle column, and also Ref. [14]). The biexciton binding energy is due to Coulomb and exchange interactions of the carriers involved. These interactions are predicted to be dependent on the microscopic distribution of As atoms in the dilute InAsP quantum dots [30], giving rise to the observed distribution of binding energies from 2.9 to −0.3 meV.

A small number of spectra consist of only a single peak [e.g., black curve in Fig. 1(c)] with a structure that shows little dependence on excitation power. Such spectra may correspond to dots which emit predominantly from the neutral exciton with biexciton emission that is energy degenerate with that of the exciton (i.e., $E_B = 0$). The latter contention is based on the observation of both positive and negative biexciton binding energies (i.e., the distribution of binding energies includes zero). Figure 2(b) shows another example of a spectrum dominated by a single resolution-limited peak (see inset) and a structure that is largely independent of excitation power. For comparison, in Fig. 2(a) we plot the pump-power-dependent emission from a dot with a nondegenerate $XX - X$ cascade which shows the expected linear (quadratic) power dependence of X [XX; see also Fig. 2(c)].
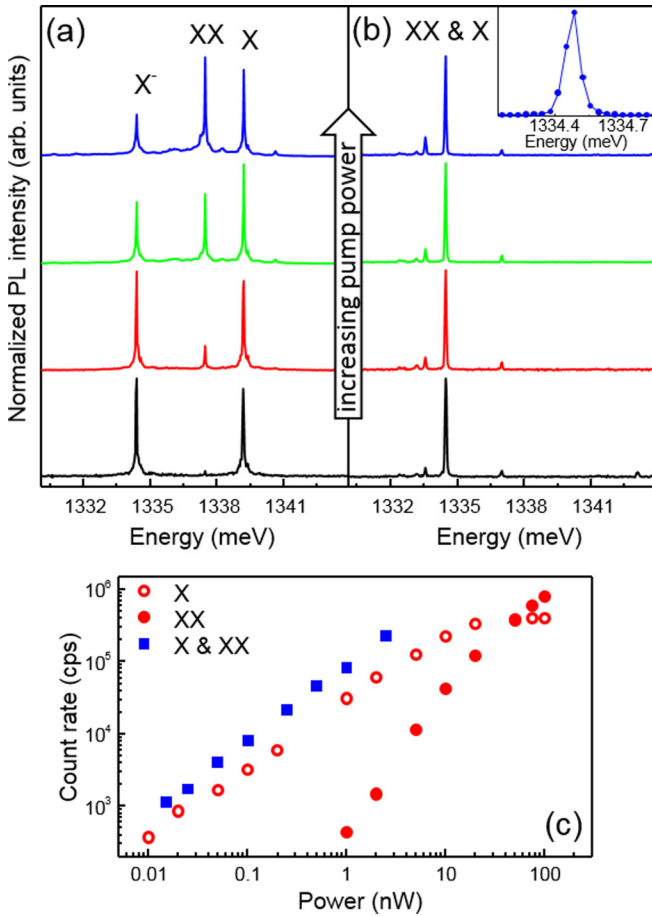
FIG. 2. Excitation-power-dependent PL spectra normalized to the X line using cw excitation for a quantum dot with (a) $E_B > 0$ and (b) $E_B = 0$. Inset: high-excitation-power spectrum over a narrow spectral range showing the resolution-limited linewidth of 60 μeV. (c) Open (solid) red circles show the linear (quadratic) power dependence of X (XX) from (a). Blue squares show the power dependence of the degenerate $X - XX$ system in (b).

To confirm that the emission peak observed in Fig. 2(b) corresponds to a degenerate $XX - X$ cascade, we have measured the second-order photon correlations $g^{(2)}(\tau)$, where $\tau = t_2 - t_1$ is the delay between the detector start (t_1) and stop (t_2) clicks. The peak at 1333.5 meV was selected using the 2-nm bandpass filter and directed to the input ports of the two APDs via a beam splitter. The second-order photon correlations as a function of pump power using cw excitation are shown in Fig. 3(b). At high excitation rates the emission is antibunched, with $g^{(2)}(0)$ as low as 0.39. As the pump power is reduced, the emission becomes bunched, with $g^{(2)}(0)$ as high as 17 for the lowest powers used (see the inset). This behavior is in strong contrast to the photon correlations measured on photons from a single decay process (X or X^-) in a nondegenerate system such as that shown in Fig. 3(a). In this case, the emission is antibunched for all excitation powers; varying the power changes only the width of the dip at $\tau = 0$ and the amount of bunching at short delays, as discussed below.

A similar excitation-rate-mediated transition from antibunched to bunched statistics for the degenerate $XX - X$ cascade is observed using pulsed excitation and is shown in
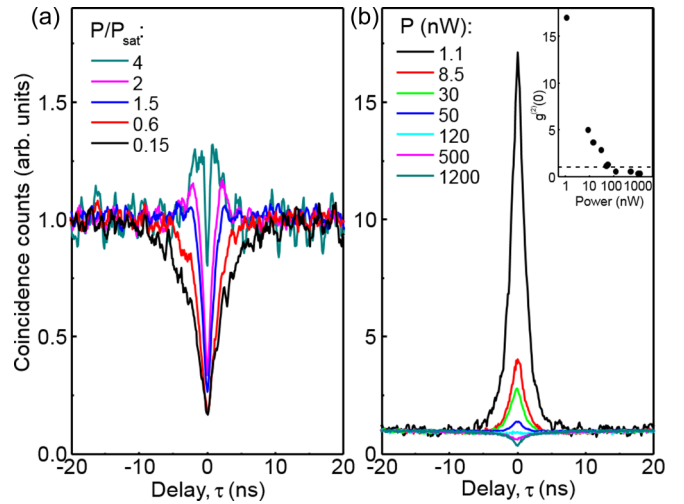
FIG. 3. Power-dependent photon correlation histograms using cw excitation for (a) X photons from a quantum dot with a nondegenerate $XX - X$ cascade, $E_B \neq 0$, and (b) X and XX photons from a dot with $E_B = 0$. The inset shows $g^{(2)}(0)$ as a function of pump power, where the dashed horizontal line indicates $g^{(2)}(0) = 1$. In (a) the pump power P is given as a fraction of the power required to saturate the X transition P_{sat}.

Fig. 4. In this case, the power-dependent statistics are quantified by the area ratio of the zero-delay peak to the side peaks $g^{(2)}(\delta\tau_p)$ and is shown in the inset. As with cw excitation, at low excitation rates the emission is bunched, with values approaching $g^{(2)}(\delta\tau_p) = 30$, and becomes antibunched as the pump rate is increased, with values of $g^{(2)}(\delta\tau_p) = 0.5$ in the high-pump limit.

The bunching observed at low excitation rates for both cw and pulsed excitation is a signature of twin-photon emission
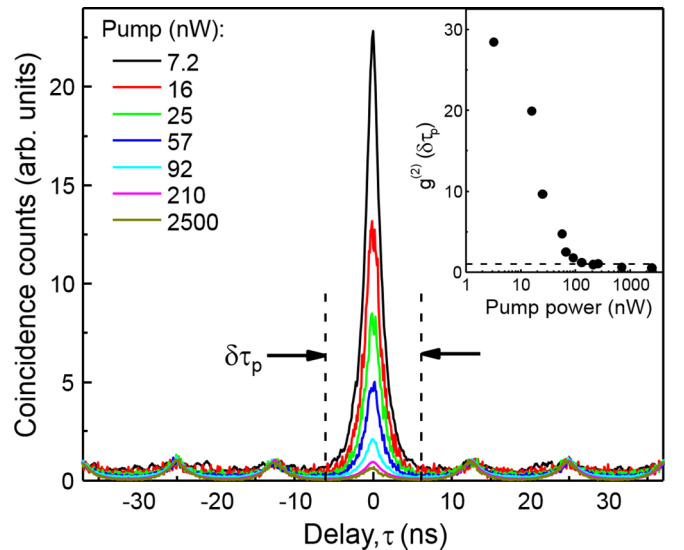
FIG. 4. Power-dependent autocorrelation measurements using pulsed excitation at a repetition rate of 80 MHz. The inset shows the intensity in the zero-delay peak normalized to the side peaks $g^{(2)}(\delta\tau_p)$ as a function of pump power, with the dashed horizontal line indicating a value of 1.

from a degenerate $XX - X$ cascade and was previously observed in other quantum dot systems [7,31,32]. Although the bunching value does not carry information about the photon pair generation efficiency, as discussed in Ref. [7], it does depend on the occupation of the exciton level: lower average probabilities of dot occupation (i.e., lower excitation rates) result in higher bunching values (see, for example, Kuroda *et al.* [33] in relation to cross-correlation measurements). Our observation of unprecedentedly strong bunching instead implies a high collection efficiency from the source, allowing us to access lower excitation levels while maintaining a good signal-to-noise ratio. This suggests that there is no fundamental limit on the bunching value other than the signal-to-noise ratio. The high bunching value also implies a high degree of degeneracy between X and XX as any deviations from a strictly resonant cascade are expected to reduce the amount of bunching [31].

The transition from strongly bunched to antibunched statistics with increasing excitation power has, to our knowledge, not been previously reported. Other power-dependent correlation measurements on degenerate $XX - X$ cascades using cw excitation [7,31] have shown only a limited dependence of $g^{(2)}(0)$ on power, with values of 3 to 5 at low excitation rates, decreasing to ~ 1 at high rates. Below (see Sec. IV) we compare the observed power-dependent photon statistics with the predictions of two models. For cw excitation, we use a four-level rate equation model, while for pulsed excitation we perform simulations using a stochastic model of the emission and detection process.

IV. MODELING

To account for the power-dependent correlations observed using cw excitation, we model the quantum dot using the theoretical description given in Ref. [7]. The dot is modeled as a four-level system consisting of the vacuum state, two bright exciton states, and the biexciton state. The time evolution of the occupation probability of the different states is derived from the system of differential equations corresponding to the four-level model (see, for example, Refs. [4,34]). The equations include transitions which increase the number of excitons in a particular state driven by a pump rate R and dependent on the occupation of the lower level. Radiative recombination processes that decrease state occupation are characterized by exciton and biexciton lifetimes of $\tau_x = 1$ ns and $\tau_{xx} = 0.5$ ns, respectively, which are typical in the InAsP/InP nanowire quantum dot system [15,16]. These equations and the corresponding two-photon correlations $g^{(2)}_{ij}(\tau)$ ($i = X, XX$, $j = X, XX$) are given in the Supplementary Information of Ref. [7].

The calculated pump-rate-dependent two-photon correlations of the four possible detection sequences are shown in Fig. 5. The top two panels show the calculated power-dependent correlations between photons produced from the same decay process (i.e., true autocorrelations $g^{(2)}_{x,x}$ and $g^{(2)}_{xx,xx}$). In the case of X photons the calculated coincidence curve reflects the probability of detecting an exciton photon at t_2 given that an exciton photon was detected at t_1 (which left the dot empty). For exciton pump rates below saturation, the calculated correlations reproduce the behavior typically
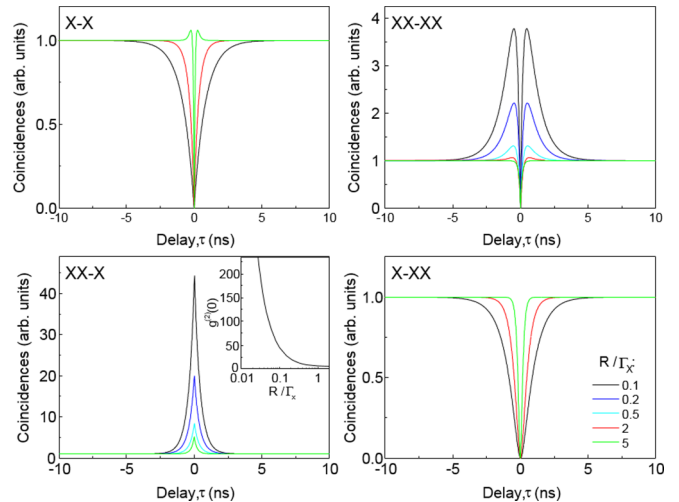
FIG. 5. Calculated second-order correlations $g^{(2)}_{ij}(\tau)$ corresponding to each of the decay processes present in a degenerate $XX - X$ system using $\tau_x = 1$ ns and $\tau_{xx} = 0.5$ ns. Pump rates R are normalized to the exciton recombination rate $\Gamma_x = 1/\tau_x$. The inset in the bottom left panel shows $g^{(2)}(0)$ as a function of pump rate.

described by a two-level model consisting of only the vacuum and exciton states, for which $g^{(2)}(\tau) = 1 - e^{-(R+\Gamma_x)|\tau|}$. This model predicts an antibunching dip with a width that reflects the exciton lifetime when $R \ll \Gamma_x$ while for $R \gg \Gamma_x$, the width is limited by the excitation rate. This narrowing of the antibunching dip with increasing excitation rate is visible in the measured correlations of X photons in the nondegenerate system shown in Fig. 3(a).

For pump rates above saturation, the probability of loading the dot with two electron-hole pairs increases, and the appropriate model requires the inclusion of an additional level to account for the biexciton (see, for example, Refs. [4,35]). Increasing the probability of populating the dot with two electron-hole pairs leads to a reduction in the average probability of observing an X photon since the dot may be repopulated with a second pair prior to X photon emission. However, at short delays (i.e., right after detection of the start photon), the dot is necessarily empty, and therefore, the probability of observing an X photon is higher compared to the average. This gives rise to the bunching calculated for short delays and is also observed experimentally in the nondegenerate system shown in Fig. 3(a) (see also Ref. [36]).

In contrast to the $X - X$ autocorrelations, the $XX - XX$ autocorrelations show short-delay bunching at *low* excitation rates, implying that a stop XX photon is more likely for short delays in comparison to long delays [37]. After the detection of the initial XX start photon, the dot is necessarily occupied by a single exciton. The short-delay XX detection process would then correspond to the capture of a second electron-hole pair by the dot followed by XX stop emission, a far more likely process than the long-delay alternative, which would correspond to the decay of the exciton to vacuum followed by the capture of two electron-hole pairs by the dot.

In addition to the true autocorrelations above, in the $XX - X$ cascade both X and XX produce detector clicks, so both $g^{(2)}_{xx,x}$ and the time-inverted $g^{(2)}_{x,xx}$ need to be considered. These
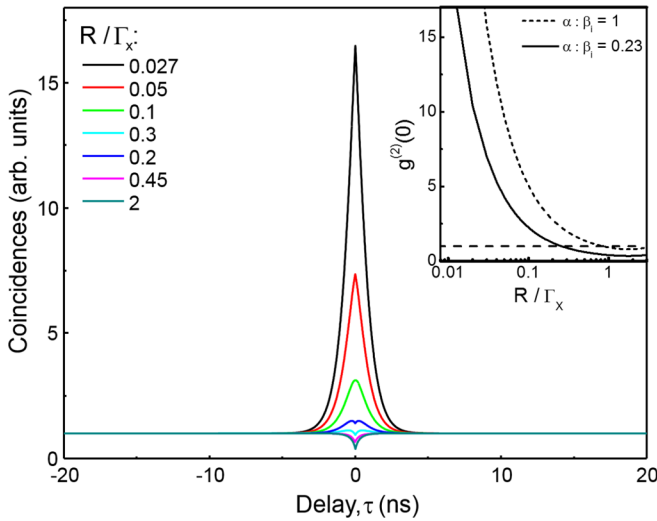
FIG. 6. Calculated pump-rate-dependent $g_T^{(2)}(\tau)$ for cw excitation using a four-level rate equation model where 7% of the decay processes are attributed to an $XX - X$ cascade. The inset shows the calculated dependence of $g_T^{(2)}(0)$ on excitation rate when 7% of the decay processes are attributed to an $XX - X$ cascade (solid line) compared to all four processes equally weighted (short-dashed line). The horizontal dashed line indicates $g^{(2)}(0) = 1$.

FIG. 7. Simulated power-dependent correlations for pulsed excitation from a three-level stochastic model using $P_{xx} = 1$. The inset shows the power-dependent coincidence counts in the zero-delay peak normalized to the side peaks $g^{(2)}(\delta\tau_p)$ using $P_{xx} = P_x$ (open circles) and $P_{xx} = 1$ (solid circles) while the dashed horizontal line indicates a value of 1.

correlations are shown in the bottom two panels of Fig. 5. The $g_{xx,x}^{(2)}$ term represents the two-photon decay process that produces photon pairs. Of the four correlations in Fig. 5, $g_{xx,x}^{(2)}$ is the only one not equal to zero at $\tau = 0$; for the other three cases the dot has to be refilled with either one or two electron-hole pairs to produce a stop click. Therefore, of the four possible decay processes that may occur in the $XX - X$ cascade, any counts at $\tau = 0$ must be due to $g_{xx,x}^{(2)}$. The calculated pump-rate-dependent $g_{xx,x}^{(2)}(0)$ is shown in the inset of the bottom left panel in Fig. 5. The model predicts a $g_{xx,x}^{(2)}(0) \sim 5.2$ at a pump rate of $\sim 2\Gamma_x$ which increases by a factor of ~ 45 as the pump rate is reduced by two orders of magnitude, similar to what is observed experimentally [see inset in Fig. 3(b)].

In the measurement of the correlations of the degenerate $XX - X$ system, all four correlations in Fig. 5 are superimposed to give the observed correlation behavior $g_T^{(2)} = \alpha g_{xx,x}^{(2)} + \beta_1 g_{xx,xx}^{(2)} + \beta_2 g_{x,x}^{(2)} + \beta_3 g_{x,xx}^{(2)}$. In our calculations, we have set the fraction of all processes that do not contribute counts at zero delay equal (i.e., $\beta_1 = \beta_2 = \beta_3$). Since there is no information in the measured correlation spectra to distinguish between each of these processes, this choice is arbitrary and chosen for simplicity. In contrast, $g^{(2)}(0)$ is sensitive to the ratio $\alpha{:}\beta_i$ with lower values predicted as $\alpha{:}\beta_i$ is reduced. For example, in the inset in Fig. 6 we compare the case where all four process are equally weighted (i.e., $\alpha{:}\beta_i = 1$), with $\alpha{:}\beta_i = 0.23$ (i.e., $\sim 7\%$ of all decay processes correspond to an $XX - X$ cascade). The latter ratio is chosen since it best reproduces the experimentally observed dependence of the zero-delay coincidence counts on excitation rate, e.g., from $g^{(2)}(0) = 0.39$ to $g^{(2)}(0) = 17$ for a 100-fold decrease in pump rate (see the inset in Fig. 3). Using $\alpha{:}\beta_i = 0.23$ also reproduces the temporally resolved experimental coincidence curves $g_T^{(2)}(\tau)$ and their dependence on excitation power

(compare Figs. 3 and 6). We note that the good correspondence between theory and experiment is achieved using a pump-independent $\alpha{:}\beta_i$ ratio, which is likely not the case (see Ref. [7]).

To account for the pump-rate-dependent correlations observed using pulsed excitation, we use a stochastic model to describe the excitonic emission and detection processes [38]. Exciton complexes are created by a continuous train of pump pulses with a given period, followed by biexciton/exciton emission at a time determined by a random number selected from a distribution weighted with the appropriate excitonic lifetime. The model assumes three possible states for the system: vacuum (no excitons created), a single exciton, or a biexciton. The resulting biexciton, exciton, vacuum decay cascade leads to photon emission and detection at times which are stored, and the process is repeated through the pulse train until a sufficiently accurate time distribution can be obtained. The completed detection time stream is allocated by random selection into start and stop detector streams. In the model we assume that there is no reexcitation of the dot between pump pulses.

In the model, the pump rate is controlled by adjusting the probability P_x of elevating the system from the vacuum to the exciton state. For consistency with the rate equation model, we set the probability of elevating the system from the exciton state to the biexciton state P_{xx}, which is contingent on the occupation of the X state, equal to P_x. The normalized coincidence count rate in the zero-delay peak $g^{(2)}(\delta\tau_p)$ calculated using $P_{xx} = P_x$ is shown in the inset in Fig. 7. Using these excitation conditions, the model drastically underestimates the bunching compared to experiment, predicting a $g^{(2)}(\delta\tau_p)$ that asymptotically approaches ~ 2 in the low-pump-rate limit.

In order to obtain agreement with experiment, we are required to assume that once in the exciton state, excitation to the biexciton state via electron-hole capture from the band

is guaranteed. In other words, the probability of producing a biexciton given that an exciton is already present P_{xx} is set equal to 1. In Fig. 7 we show the calculated, power-dependent correlations predicted using the condition $P_{xx} = 1$. The calculated correlations reproduce the measured spectra in Fig. 4 and predict a normalized coincidence count rate in the zero-delay peak $g^{(2)}(\delta\tau_p) = 0.5$ when $P_x = 1$, which increases to 25 as P_x is decreased by a factor of 50, similar to that observed experimentally (compare the insets in Figs. 4 and 7).

V. DISCUSSION

In the rate equation model we have assumed that the ratio $\alpha : \beta_i$ is independent of pump power. With this assumption, the value of the ratio is well constrained if the intent is for the model to reproduce the experimental data over a wide range of pump powers. The ratio $\alpha : \beta_i$, however, is likely to depend on the excitation power, and previous experiments suggest that the efficiency of the process responsible for generating photon twins, represented by α, increases relative to the other processes as the pump power is increased [7]. Introducing a pump power dependence in $\alpha : \beta_i$ would remove constraints on the solution and allow for the calculation of a much wider range of possible bunching values.

The stochastic model, on the other hand, is more constrained, having no input for manipulating the prevalence of any one particular decay process. In order to reproduce the experimental results using this model, a much higher than expected occupancy of the biexciton state is required. There is no clear explanation, however, as to why an artificially high occupancy of the biexciton state would arise.

The inability to reproduce the experimental data using realistic parameters implies that the existing models do not include all the physics present in a degenerate quantum dot system. In particular, neither the rate equation model nor the stochastic model explicitly contains a dependence of the bunching on the biexciton binding energy: both would predict the identical results irrespective of the value of E_B. We have, however, observed the reported high level of bunching only in quantum dots with negligible values of E_B. Indeed, as described in Ref. [31], the bunching is expected to increase in a strictly resonant system as correlated two-photon intermediate states become resonant, increasing the number of decay channels that allow for the formation of photon pairs. These additional two-photon decay processes, which contribute uniquely in degenerate systems, may account for the power-dependent bunching observed in this work.

VI. CONCLUSION

In summary, we have reported on highly symmetric (i.e., low FSS) InAs/InP nanowire quantum dots with biexciton binding energies in the range $E_B = -0.3$ to 2.9 meV. For a quantum dot with no biexciton binding energy (within the resolution of our system), we have used correlation measurements to demonstrate an excitation-rate-mediated transition from sub- to super-Poissonian statistics as the pump power is reduced. This behavior was interpreted using a four-level rate equation model and simulations based on a stochastic model of the emission and detection process. These findings demonstrate the potential of nanowire-based quantum dots as a viable route for the efficient generation of photon twins.

ACKNOWLEDGMENT

[1] J.-M. Gérard and B. Gayral, J. Lightwave Technol. **17**, 2089 (1999).

[2] P. Michler, A. Kiraz, C. Becher, W. V. Schoenfeld, P. Petroff, L. Zhang, E. Hu, and A. Imamoglŭ, Science **290**, 2282 (2000).

[3] C. Santori, D. Fattal, J. Vučković, G. Solomon, and Y. Yamamoto, Nature (London) **419**, 594 (2002).

[4] E. Moreau, I. Robert, L. Manin, V. Thierry-Mieg, J. M. Gérard, and I. Abram, Phys. Rev. Lett. **87**, 183601 (2001).

[5] O. Benson, C. Santori, M. Pelton, and Y. Yamamoto, Phys. Rev. Lett. **84**, 2513 (2000).

[6] R. M. Stevenson, R. J. Young, P. Atkinson, K. Cooper, D. A. Ritchie, and A. J. Shields, Nature (London) **439**, 179 (2006).

[7] T. Heindel, A. Thoma, M. von Helversen, M. Schmidt, A. Schlehahn, M. Gschrey, P. Schnauber, J.-H. Schulze, A. Strittmatter, J. Beyer, S. Rodt, A. Carmele, A. Knorr, and S. Reitzenstein, Nat. Commun. **8**, 14870 (2017).

[8] R. Seguin, A. Schliwa, S. Rodt, K. Pötschke, U. W. Pohl, and D. Bimberg, Phys. Rev. Lett. **95**, 257402 (2005).

[9] R. J. Young, R. M. Stevenson, A. J. Shields, P. Atkinson, K. Cooper, D. A. Ritchie, K. M. Groom, A. I. Tartakovskii, and M. S. Skolnick, Phys. Rev. B **72**, 113305 (2005).

[10] M. E. Reimer, D. Dalacu, J. Lapointe, P. J. Poole, D. Kim, G. C. Aers, W. R. McKinnon, and R. L. Williams, Appl. Phys. Lett. **94**, 011108 (2009).

[11] S. Seidl, M. Kroner, A. Högele, K. Karrai, R. Warburton, A. Badolato, and P. M. Petroff, Appl. Phys. Lett. **88**, 203113 (2006).

[12] M. Borgström, V. Zwiller, E. Müller, and A. Imamoglu, Nano Lett. **5**, 1439 (2005).

[13] P. M. Petroff and S. P. DenBaars, Superlattices Microstruct. **15**, 15 (1994).

[14] D. Dalacu, K. Mnaymneh, J. Lapointe, X. Wu, P. J. Poole, G. Bulgarini, V. Zwiller, and M. E. Reimer, Nano Lett. **12**, 5919 (2012).

[15] M. E. Reimer, G. Bulgarini, A. Fognini, R. W. Heeres, B. J. Witek, M. A. M. Versteegh, A. Rubino, T. Braun, M. Kamp, S. Höfling, D. Dalacu, J. Lapointe, P. J. Poole, and V. Zwiller, Phys. Rev. B **93**, 195316 (2016).

[16] M. A. M. Versteegh, M. E. Reimer, K. D. Jöns, D. Dalacu, P. Poole, A. Gulinatti, A. Giudice, and V. Zwiller, Nat. Commun. **5**, 6298 (2014).

[17] T. Huber, A. Predojević, M. Khoshnegar, D. Dalacu, P. Poole, H. Majedi, and G. Weihs, Nano Lett. **14**, 7107 (2014).

[18] M. Khoshnegar, T. Huber, A. Predojević, D. Dalacu, M. Prilmüller, J. Lapointe, X. Wu, P. Tamarat, B. Lounis, P. Poole, G. Weihs, and H. Majedi, Nat. Commun. **8**, 15716 (2017).

[19] S. Haffouz, K. D. Zeuner, D. Dalacu, P. J. Poole, J. Lapointe, D. Poitras, K. Mnaymneh, X. Wu, M. Couillard, M. Korkusinski,

E. Schöll, K. D. Jöns, V. Zwiller, and R. L. Williams, Nano Lett. **18**, 3047 (2018).

[20] A. Fiset-Cyr, D. Dalacu, S. Haffouz, P. J. Poole, J. Lapointe, G. C. Aers, and R. L. Williams, Appl. Phys. Lett. **113**, 053105 (2018).

[21] M. E. Reimer, M. P. van Kouwen, A. W. Hidma, M. H. M. van Weert, E. P. A. M. Bakkers, L. P. Kouwenhoven, and V. Zwiller, Nano Lett. **11**, 645 (2011).

[22] K. Lagoudakis, P. McMahon, C. Dory, K. Fischer, K. Müller, V. Borish, D. Dalacu, P. Poole, M. Reimer, V. Zwiller, Y. Yamamoto, and J. Vučković, Optica **3**, 1430 (2016).

[23] Y. Chen, I. E. Zadeh, K. D. Jöns, A. Fognini, M. E. Reimer, J. Zhang, D. Dalacu, P. J. Poole, F. Ding, V. Zwiller, and O. G. Schmidt, Appl. Phys. Lett. **108**, 182103 (2016).

[24] M. Korkusinski, M. E. Reimer, R. L. Williams, and P. Hawrylak, Phys. Rev. B **79**, 035309 (2009).

[25] M. Bayer, G. Ortner, O. Stern, A. Kuther, A. A. Gorbunov, A. Forchel, P. Hawrylak, S. Fafard, K. Hinzer, T. L. Reinecke, S. N. Walck, J. P. Reithmaier, F. Klopf, and F. Schäfer, Phys. Rev. B **65**, 195315 (2002).

[26] D. Dalacu, A. Kam, D. G. Austing, X. Wu, J. Lapointe, G. C. Aers, and P. J. Poole, Nanotechnology **20**, 395602 (2009).

[27] N. Gregersen, T. R. Nielsen, J. Claudon, J.-M. Gérard, and J. Mørk, Opt. Lett. **33**, 1693 (2008).

[28] J. Claudon, J. Bleuse, N. S. Malik, M. Bazin, P. Jaffrennou, N. Gregersen, C. Sauvan, P. Lalanne, and J.-M. Gérard, Nat. Photonics **4**, 174 (2010).

[29] R. Singh and G. Bester, Phys. Rev. Lett. **103**, 063601 (2009).

[30] M. Cygorek, M. Korkusinski, and P. Hawrylak, Phys. Rev. B **101**, 075307 (2020).

[31] G. Callsen, A. Carmele, G. Hönig, C. Kindel, J. Brunnmeier, M. R. Wagner, E. Stock, J. S. Reparaz, A. Schliwa, S. Reitzenstein, A. Knorr, A. Hoffmann, S. Kako, and Y. Arakawa, Phys. Rev. B **87**, 245314 (2013).

[32] S. Moroni, S. Varo, G. Juska, T. Chang, A. Gocalinska, and E. Pelucchi, J. Cryst. Growth **506**, 36 (2019).

[33] T. Kuroda, T. Belhadj, M. Abbarchi, C. Mastrandrea, M. Gurioli, T. Mano, N. Ikeda, Y. Sugimoto, K. Asakawa, N. Koguchi, K. Sakoda, B. Urbaszek, T. Amand, and X. Marie, Phys. Rev. B **79**, 035330 (2009).

[34] G. Sek, A. Musial, P. Podemski, and J. Misiewicz, J. Appl. Phys. **108**, 033507 (2010).

[35] J. Szeszko, V. V. Belykh, A. Rudra, B. Dwir, N. N. Sibeldin, and E. Kapon, Phys. Rev. B **91**, 245304 (2015).

[36] D. V. Regelman, U. Mizrahi, D. Gershoni, E. Ehrenfreund, W. V. Schoenfeld, and P. M. Petroff, Phys. Rev. Lett. **87**, 257401 (2001).

[37] A. Kiraz, S. Fälth, C. Becher, B. Gayral, W. V. Schoenfeld, P. M. Petroff, L. Zhang, E. Hu, and A. Imamoglŭ, Phys. Rev. B **65**, 161303(R) (2002).

[38] K. Mnaymneh, D. Dalacu, J. McKee, J. Lapointe, S. Haffouz, J. F. Weber, D. B. Northeast, P. J. Poole, G. C. Aers, and R. L. Williams, Adv. Quantum Technol. **3**, 1900021 (2020).